



HAL
open science

Complex coacervation of pea protein isolate and tragacanth gum: Comparative study with commercial polysaccharides

Jérémy Carpentier, Egle Conforto, Carine Chaigneau, Jean-Eudes Vendeville,
Thierry Maugard

► To cite this version:

Jérémy Carpentier, Egle Conforto, Carine Chaigneau, Jean-Eudes Vendeville, Thierry Maugard. Complex coacervation of pea protein isolate and tragacanth gum: Comparative study with commercial polysaccharides. *Innovative Food Science & Emerging Technologies / Innovative Food Science and Emerging Technologies*, 2021, 69, pp.102641. 10.1016/j.ifset.2021.102641 . hal-03501536

HAL Id: hal-03501536

<https://univ-rochelle.hal.science/hal-03501536v1>

Submitted on 10 Mar 2023

HAL is a multi-disciplinary open access archive for the deposit and dissemination of scientific research documents, whether they are published or not. The documents may come from teaching and research institutions in France or abroad, or from public or private research centers.

L'archive ouverte pluridisciplinaire **HAL**, est destinée au dépôt et à la diffusion de documents scientifiques de niveau recherche, publiés ou non, émanant des établissements d'enseignement et de recherche français ou étrangers, des laboratoires publics ou privés.



Distributed under a Creative Commons Attribution - NonCommercial 4.0 International License

1 **Complex coacervation of pea protein isolate and tragacanth gum: comparative study with**
2 **commercial polysaccharides.**

3

4 Jérémy CARPENTIER ^{a,c}, Egle CONFORTO ^b, Carine CHAIGNEAU ^c, Jean-Eudes VENDEVILLE ^c, Thierry
5 MAUGARD ^a

6

7 ^a Université de La Rochelle, UMR CNRS 7266, LIENSs, UFR Sciences, Avenue Michel Crépeau, 17042 La
8 Rochelle, FRANCE

9 ^b Université de La Rochelle, UMR CNRS 7356, LaSIE, UFR Sciences, Avenue Michel Crépeau, 17042 La
10 Rochelle, FRANCE

11 ^c IDCAPS, filiale R&D INNOV'IA, 4 rue Samuel Champlain, Z.I. Chef de Baie, 17000 La Rochelle, FRANCE

12

13

14 *Author to who correspondence should be addressed

15 E-mail: thierry.maugard@univ-lr.fr

16 Phone : +33 5 16 49 82 77

17

18

19 **Key Words**

20 Pea Protein Isolate, Tragacanth gum, Complex coacervates, Protein-polysaccharide interaction, Zeta
21 potential, Solubility

22

23

24

25

26

27

28

29

30

31

32

33

34 **Abstract**

35 The ability of pea protein isolates (PPI) to form complex coacervates with tragacanth gum was
36 investigated. The coacervate formation was structurally compared to three other PPI-polysaccharide
37 interaction models: arabic gum and sodium alginate (known to form coacervates with PPI) and tara
38 gum, a galactomannan. The effects of the pH and protein/polysaccharide ratio were mainly
39 investigated using turbidity and zeta potential measurements. Regarding the pH of soluble complex
40 formation, the pH of complex coacervates increased with the increase in protein-anionic
41 polysaccharide mixture ratio. SEM images revealed the ability of the spray-drying process to form
42 spherical particles of pea protein-polysaccharide complexes. The specificity of the microparticle
43 surface was protein-dependent. FTIR analyses of coacervates showed the electrostatic interaction
44 between the PPI and the polysaccharides. The results showed that tragacanth gum could be used as
45 an alternative to gum arabic to form complex coacervates with PPI based on zeta potential
46 measurements and coacervation yield studies.

47

48

49

50

51

52

53

54

55

56

57

58

59

60

61

62

63

64

65

66

67

68

70 1. Introduction

71 For a few years, plant proteins were of a growing interest for ingredient industry as an alternative to
72 animal sources (gelatin, whey, casein) due to safety concerns (Toews and Wang, 2013). Among plant
73 proteins, yellow pea (*Pisum sativum L.*) protein isolates (PPI) represent attractive hydrocolloids in
74 food and nutraceutical applications due to their health benefits, their allergen and gluten-free
75 properties, a wide availability and low price. The composition of pea proteins is mainly comprised of
76 albumin (10-20% of total proteins) and of two major globulin proteins (70-80% of the total proteins):
77 legumin (11S; 350–400kDa), vicilin and convicilin (7S; 150 and 290kDa respectively) (Adebiyi and
78 Aluko, 2011). Pea protein contains a wide range of charged amino acids, especially lysine ($\approx 6\%$),
79 aspartic acid ($\approx 11\%$), glutamic acid ($\approx 17\%$), arginine ($\approx 7\%$), leucine ($\approx 7\%$) in its polypeptide chains
80 exhibiting the polyelectrolyte nature of pea proteins (Boye et al., 2010).

81 The establishment of interaction between proteins and polysaccharides lead to the formation of
82 complexes that can improve the functionalities of proteins to stabilize emulsions and foams (Tamnak
83 et al., 2016), control the structure and texture of foods and biomaterials (Turgeon et al., 2003), or to
84 design carrier vehicles in the protection and delivery of active compounds to targeted sites and
85 improve their bioavailability (Jain et al., 2016). The complex coacervation, also known as an
86 associative phase separation, is characterized by an electrical balance between two oppositely
87 charged polyelectrolytes (such as a protein, polysaccharide) in aqueous media. Two phases are thus
88 obtained: a biopolymer rich phase and a solvent rich phase. This phenomenon depends on the
89 conditions such as the pH, charge density and molecular weight of the related polymers, the colloid
90 concentration, temperature and ionic strength of media, etc. (Turgeon et al., 2003; Weinbreck et al.,
91 2003). Not all polyelectrolytes are subject to this phenomenon. Complex coacervation is a
92 thermodynamic phenomenon that can be driven enthalpically or entropically by driving forces such
93 as electrostatic interactions or counterion release, with contributions from hydrogen bonding and
94 hydrophobic interactions (Kayitmazer, 2017).

95 Three critical structure-forming events (pH_c , pH_{ϕ_1} , pH_{ϕ_2}) have been defined based on the changes in
96 turbidity curves during the titration from alkaline to acidic pH (Liu et al., 2009). These events
97 correspond to four different phase behaviors: the co-solubility of biopolymers ($pH > pH_c$), the
98 formation of soluble complexes ($pH_c > pH > pH_{\phi_1}$), the formation of complex coacervates inducing a
99 strong increase in turbidity ($pH_{\phi_1} > pH > pH_{\phi_2}$), and the dissolution of complexes due to the
100 protonation of reactive groups on the polysaccharide backbone ($pH < pH_{\phi_2}$). A maximum optical
101 density (OD), also called pH_{opt} , takes place between pH_{ϕ_1} and pH_{ϕ_2} , corresponding to the maximum
102 amount of coacervates produced at the electrical equivalence of the relevant biopolymer. It has been
103 described that from pH_{ϕ_1} to pH_{opt} the electrostatic attractive forces become stronger, reaching the
104 maximum electrostatic interaction. This event is a key factor for microencapsulation applications (de
105 Vries et al., 2003; Turgeon et al., 2003; Weinbreck et al., 2003). Controlled protein-polysaccharide
106 interactions through complex coacervation improve their functional role as ingredients, without
107 chemical modification (Nesterenko et al., 2012).

108 Many studies have been focused on the phase behavior of pea protein-polysaccharide complexes,
109 including pea protein - alginate (Klemmer et al., 2012), pea protein - pectin (Tamnak et al., 2016) or
110 pea protein - arabic gum (Liu et al., 2009). To the best of our knowledge, no study has assessed on
111 the formation of complex coacervates of pea proteins and tragacanth gum as an alternative to arabic
112 gum. Tragacanth gum is an exudate of Asian species of *Astragalus* and consists of two fractions: the
113 water-soluble fraction (composed of tragacanthin) and the water-insoluble fraction (bassorin) and

114 contain a small amount of protein (>4% w/w) (Anderson and Bridgeman, 1985). Tragacanthin, an
115 anionic component, is composed of a chain of α -(1–4)-linked D-galacturonic acid units, some of
116 which being replaced at O-3 by β -D-xylopyranosyl units and some of them being terminated with D-
117 Galactose or L-Fucose. The galacturonic acid content varies from 10 to 30% per weight in dry matter
118 depending on the species (Balaghi et al., 2010). The gum may be used in numerous applications in
119 food, pharmaceutical and cosmetic industries due to its anionic properties making it highly resistant
120 to acid environments (Nazarzadeh Zare et al., 2019). Tragacanth gum, described as a bifunctional
121 emulsifier, showed efficient acidic oil-in-water emulsions properties (Balaghi et al., 2010; Farzi et al.,
122 2013), gelling abilities and high mucoadhesive properties (Nur et al., 2016). Largely studied in
123 biomedical field, tragacanth gum was identified as non-toxic, non-teratogenic, non-carcinogenic and
124 non-mutagenic, and can be suitable in wound dressing (Ghayempour et al., 2016). It has been
125 reported to be “generally recognized as safe” by the US Food and Drug Administration (FDA) since
126 1961. Using gum tragacanth as a food additive in food preparations is permitted by the FDA Code of
127 Federal Regulations at the concentration of 0.2-1.3%wt. The Scientific committee for Food of the
128 European Community has approved the tragacanth gum as the food additive E-number E413
129 (Nazarzadeh Zare et al., 2019).

130 The aim of this study was to investigate the effect of the nature of marketed polysaccharides,
131 especially gum tragacanth, on the mechanisms determining complex coacervation with the total
132 fraction of a marketed PPI and the resulting complexation-induced changes in protein conformation
133 under optimal coacervation conditions. However, identifying the pH range for the formation of
134 complex coacervates in concentrated biopolymer systems in order to understand their phase
135 transition, structural aspects and functional properties depending on the polysaccharide structure is
136 challenging. Research work has mainly been focused on coacervate formation at concentrations less
137 than 0.3% w/v. Studying the formation of complex coacervates at higher protein concentrations
138 promoted the use of pea protein in food products.

139 In this study, particles of complex coacervates were assembled by preparing mixtures of PPI and
140 different polysaccharides: arabic gum, sodium alginate, tragacanth gum, known as anionic
141 polysaccharides and tara gum, a non-ionic polysaccharide. This work is structured around two axes of
142 the study. The primary objective was to investigate the influence of factors such as the pH and
143 biopolymer ratios on the phase behavior of PPI-polysaccharide complex coacervates, especially pea
144 protein-tragacanth gum, in order to evaluate the physicochemical properties of these coacervates at
145 a concentration of 0.3% (w/v) by turbidimetric analysis, zeta potential measurements and protein
146 solubility determination. The second objective was to study the coacervation yield of concentrated
147 coacervates (concentration of biopolymers > 1% w/v) in order to study the adaptability of the
148 process in the field of microencapsulation. Finally, Fourier transform infrared spectroscopy (FTIR) and
149 scanning electron microscopy (SEM) were used to determine the structure of dried coacervate
150 particles. The ultimate goal of this study would be to develop microcapsule systems of plant origins
151 from the complex coacervates studied.

152

153 **2. Material and methods**

154 **2.1. Materials and chemicals**

155 Pea protein is dominated by two types of globulin storage proteins: legumin (350-400 kDa) and vicilin
156 (150 kDa). Commercially available pea protein isolate (PPI, 80% protein content) in powder form was
157 purchased from Roquette (Nutralys F85M, Lestrem, FRANCE). The product composition was
158 described as: 7% of relative humidity, 80% of proteins, 3% of carbohydrates, 6% of total fat and 4% of

159 ashes. Arabic gum was kindly supplied by CNI (Rouen, FRANCE). Tragacanth gum CEROTRAG 887 was
160 purchased from C.E. Roeper GmbH (Hamburg, GERMANY). Tara gum is a galactomannan extracted
161 from the endosperm of the seed of tara shrub *Caesalpinia spinosa*. Tara gum was purchased from
162 Starlight Products (Rouen, FRANCE). The gum obtained consisted of $\geq 80\%$ of galactomannan.
163 Alginate presents a linear structure consisting of (β -1,4)-linked mannuronic and α -guluronic acids,
164 and the proportions depend on the source. Sodium alginate (MANUCOL LD) was kindly supplied by
165 FMC Biopolymer (Philadelphia, USA). All chemicals used in this study were sold as reagent grade and
166 purchased from Sigma-Aldrich (Oakville, ON, Canada).

167 **2.2. Preparation of complex coacervates and turbidimetric acid pH titration**

168 Biopolymer stock solutions were prepared by dispersing PPI, sodium alginate (ALG), arabic gum
169 (GAC), tara gum (TARA) and tragacanth gum (TRAG) powders in Milli-Q™ water, followed by stirring
170 at 500 rpm for 2 hours at room temperature (RT:21-22°C). The total fraction of the protein was used
171 for the study. No treatment was applied to separate the fractions. For ALG, TARA and TRAG, the
172 solution was maintained at 45°C to reduce its viscosity and ensure the complete dissolution of the
173 polysaccharide. All solutions were kept overnight at 4°C to facilitate protein solubility and fully
174 hydrate the polysaccharides. All solutions were prepared at a concentration of 0.5% (w/v).

175 **2.3. Turbidimetric analysis**

176 Turbidimetric acid pH titrations of homogeneous and mixed PPI and polysaccharide systems were
177 performed using Liu et al. (2009) methods with several modifications to identify critical structure-
178 forming events (pH_c , $pH_{\phi 1}$, pH_{opt} , $pH_{\phi 2}$) and biopolymer and pH conditions under which the associative
179 phase separation took place.

180 Turbidity measurements were performed at different ratios (protein-polysaccharide mixture ratios of
181 1:1, 2:1, 5:1 and 10:1) with a pH range of 7.0-1.5 using a Fluostar Omega microplate reader (BMG
182 Labtech, FRANCE) at 600 nm in 96 well microplates. Measurements were made at room temperature
183 at a total biopolymer concentration of 0.3% (w/v). Briefly, biopolymer mixtures were mixed from
184 stock solutions to achieve the expected total biopolymer concentration (0.3% w/v) (Ghorbani Gorji et
185 al., 2014) and PPI/polysaccharide ratio (1:1, 2:1, 5:1 and 10:1). Turbidimetric titration upon
186 acidification was achieved via the dropwise addition of HCl (with a gradient HCl concentration of
187 0.05M > pH 3.5; 0.5M > pH 2.5; 1M > pH 2.0). For a 10mL solution of mixture, the maximal volume of
188 HCl added was 2,0mL. The conductimetry didn't exceed 20mS.cm⁻¹. If necessary, a dropwise addition
189 of NaOH 0.5M was achieved to reached pH 7.0. Dilution effects and changes in solution conductivity
190 were considered minimal. Structure-forming transitions were measured graphically from the curve
191 according to (Weinbreck et al., 2003), whereas pH_{opt} corresponded to the maximum OD at 600 nm.
192 All measurements were made in triplicate. A homogeneous solution of PPI or polysaccharides (GAC,
193 TRAG, ALG and TARA) were used under the same solvent conditions and at a biopolymer
194 concentration of 0.3% (w/v) to compare the profiles with mixed solutions.

195 **2.4. Protein solubility determination**

196 The pH-dependence of the percentage of protein solubility of the mixture and homogeneous PPI
197 solutions was tested using the Pierce™ BCA protein assay kit (Thermo Scientific). Briefly, 20 μ L of
198 standard or a sample from the center of the supernatant of the mixture preparation were added to
199 200 μ L of BCA working reagent in a 96 well microplate. After a 30-second agitation on a plate shaker,
200 the plate was incubated at 37°C for 30 minutes. Then, the plate was cooled to room temperature and
201 the absorbance was measured at 562nm using a Fluostar Omega microplate reader (BMG Labtech,
202 FRANCE). The protein solubility was estimated as:

203
$$PS = \frac{\text{Protein concentration of supernatant}}{\text{Protein concentration of initial solution}} \times 100$$

204 **2.5. Electrophoretic mobility**

205 The electrophoretic mobility of PPI-GAC, PPI-ALG, PPI-TRAG, PPI-TARA mixtures and homogeneous
 206 biopolymer solutions was investigated according to the pH (range: 7.0 - 1.5) using a Zetasizer Nano-
 207 ZS90 (Malvern Instruments, Westborough, MA). The solution pH was decreased by 0.5 pH unit
 208 increments through the dropwise addition of hydrochloric acid (0.05M > pH7.0; 0.5M > pH 2.5).
 209 Samples were prepared as described in the section above to a final biopolymer concentration of 0.3%
 210 (w/v). Using the Henry equation, the electrophoretic mobility was used to estimate the zeta
 211 potential:

212
$$UE = \frac{2\varepsilon \times \xi \times f(\kappa\alpha)}{3\eta}$$

213 Where η is the dispersion viscosity, ε is the permittivity, $f(\kappa\alpha)$ is a function related to the ratio of
 214 particle radius (α) and the Debye length (κ). Using the Smoluchowski approximation, $f(\kappa\alpha)$ was equal
 215 to 1.5. All measurements were equilibrated at 25°C for 60s and analysed in triplicate.

216 **2.6. Coacervation yield of concentrated mixtures**

217 Mixed solutions were prepared as for the turbidimetric analysis at a total biopolymer concentration
 218 of 5.0% (w/v), except for PPI-TRAG and PPI-TARA mixtures at a ratio of 2:1 that were diluted
 219 respectively to 2% and 1% (w/v) due to the viscosity of the polysaccharide solutions (Table 1). The pH
 220 was adjusted between 2.5 and 4.5 with 0.5M HCl.

221 *Table 1: Total biopolymer concentration of the various mixed Protein-polysaccharides solutions tested*

Ratio	PPI-TRAG	PPI-GAC	PPI-ALG	PPI-TARA
2:1	2% w/v	5% w/v	5% w/v	1% w/v
5:1	5% w/v	5% w/v	5% w/v	5% w/v
10:1	5% w/v	5% w/v	5% w/v	5% w/v

222
 223 Briefly, the mixture was left for 60 minutes at room temperature, followed by centrifugation at 1,000
 224 g for 10 minutes. The volume of supernatant was recovered, and the weight of the resulting pellet
 225 after drying at 105°C in oven and supernatant was recorded. The coacervate yield was calculated as:

226
$$CY = \frac{\text{Dry weight of coacervates}}{\text{Total weight of protein, polysaccharides used in the preparation}} \times 100$$

227 The protein solubility of the mixtures was also determined using the same procedure as described
 228 above.

229 **2.7. Preparation of particles**

230 The spray-drying technology was used to prepare microparticles from feed solutions, composed of
 231 pea protein – polysaccharide complex coacervates. The solutions were prepared as follows: an
 232 amount of PPI and polysaccharide (arabic gum, sodium alginate, tragacanth gum and tara gum)
 233 powders was dissolved separately in distilled water by stirring at 500 rpm for 2 hours at room
 234 temperature. For ALG, TARA and TRAG, the solution was maintained at 45°C to reduce the viscosity
 235 of solution and ensure the complete dissolution of the polysaccharide.

236 Then the solutions of proteins and polysaccharides were mixed at a protein/polysaccharide ratio of
 237 5:1, and the pH was adjusted to the previously determined optimal value. The feed solutions were

238 dried in a Mini Spray Dryer Büchi 190 (Büchi Laboratory Equipment, Switzerland), inlet air
239 temperature at 140°C and outlet at 80°C, nozzle of 0.7 mm, and 0,4 Lh⁻¹ feed rate. The feed solution
240 was kept under low magnetic stirring at 300 rpm during the drying step. The microparticles were
241 collected from the container, closed hermetically in an opaque packaging and stored at 4°C.

242 **2.8. Fourier transformation infrared (FTIR) spectroscopy study**

243 FTIR spectra of spray-dried complexes and biopolymer powders were recorded using a Spectrum 100
244 FT-IR spectrometer (Perkin Elmer). Transmission spectra were obtained within a range of 4,000-
245 650cm⁻¹ using 32 scans at a resolution of 4 cm⁻¹. The scattering correction procedure was used to
246 correct spectra for the baseline. Mean spectra were calculated from triplicate of independent
247 measurements.

248 **2.9. ESEM morphological observations**

249 The surface morphology of the samples was monitored using an environmental scanning electron
250 microscope (ESEM) (QUANTA 200 Environmental Field Effect Gun apparatus, FEI, FRANCE). The
251 observations were made according to Conforto et al. (2015) with several changes. The particles were
252 deposited on conductive carbon double-faced adhesive tape on aluminum SEM stubs. As described
253 by the author, no coating was applied to the samples before the observation in order to avoid any
254 alteration of the particle surface. The analyses were performed in environmental mode under water
255 vapor pressure with a beam current between 0.1 and 2 nA and an accelerating voltage in the 11-20
256 kV range. Secondary electron (SE) images were obtained using a Large-Field (LFD) detector. Details of
257 the surface morphology were obtained by varying the water vapor pressure within the 1.20-1.30
258 mbar range as well as the accelerating voltage of the primary beam.

259 **2.10. Statistical analysis**

260 All measurements were carried out at least in triplicate using freshly prepared samples and data
261 were reported as mean and standard deviation.

262 **3. Results and discussion**

263 **3.1. Investigation of the protein-polysaccharide interaction by optical density measurement**

264 The effect of the pH 7.00-1.50) and biopolymer mixture ratio (1:1 – 10:1) on the complex formation
265 were investigated in admixtures of PPI and separately four different polysaccharides (ALG, GAC,
266 TRAG and TARA) at a constant total biopolymer concentration of 0.3% (w/v) by OD measurements. A
267 comparative study was shown in **figure 1A** for the 2:1 ratio of each PPI-polysaccharide mixture. OD
268 curves of the mixture supernatant compared to the OD of the homogeneous protein solution are
269 shown in **Figure 7 (supplemental data)**.

270 The homogeneous PPI system has been described in the literature as a bell-shaped turbidity curve
271 according to the pH, where OD starts to increase at a pH of about 6.50 and reaches a maximum OD
272 between pH 3.30 and 4.30, where a flattening of the curve top occurs, related to protein self-
273 aggregation. OD decreases at pH 1.70 (Klemmer et al., 2012). (**Figure 1A**).

274 The absorbance of PPI-TRAG mixtures revealed a different profile from that of PPI and TRAG
275 homogeneous solutions alone, suggesting an interaction between the protein and the
276 polysaccharide. (**Figure 7A**). The turbidity of a homogeneous tragacanth gum solution did not change
277 as a function of pH as confirmed by the literature (Ghorbani Gorji et al., 2014; Jain et al., 2016).
278 Mixed PPI-TRAG complexes at a ratio of 2:1 formed at pH 5.54 (referred to as pH_c), leading to a slight
279 increase in OD under acidification (**Figure 1A**). Interactions between PPI and TRAG are assumed to

280 take place between the negative charges of the carboxylic acid groups of TRAG chains and the
281 positively charged patches on PPI surface. The presence of TRAG caused a shift in turbidity curves
282 towards lower pH values compared to PPI alone by reducing the PPI-PPI aggregation. The pH_c
283 became ratio-independent for ratio ranging between 1:1 and 10:1 (**Figure 7A**). With further
284 acidification, the complexes with a ratio of 2:1 tended to grow at pH 4.94, resulting in the formation
285 of insoluble complexes (referred to the second critical pH parameter pH_{ϕ_1}). At this point, the OD
286 strongly increased, switching from a transparent to a cloudy dispersion (**Figure 1C**). It increased
287 curvilinearly and a shift of pH_{ϕ_1} value was observed with the increase in mixture ratio from pH 4.80-
288 5.10 at a ratio of 1:1 to pH 6.30-6.70 at the mixture ratio of 10:1 (**Figure 7A**) (Lan et al., 2020). This
289 phenomenon was attributed to the rise of self-PPI aggregates formation by increasing the protein
290 concentration in the biopolymer mixture. The turbidity further increased until reaching a maximum
291 OD at pH_{opt} (pH 4.54). At this pH value, an overall charge neutralization was supposed to occur in the
292 biopolymer mixture. At pH_{opt} , the mixtures contained the maximum amount of coacervates and thus
293 showed the maximum OD. Then, a decreasing of OD occurred with further acidification. As for pH_{ϕ_1} ,
294 pH_{opt} increased with the increase in mixture ratio. Overall, a shift of coacervation events towards
295 higher pHs was observed as the biopolymer mixture ratio increased (pH 4.49 at a ratio of 1:1 to pH
296 4.92 at a ratio of 10:1) (**Figure 1B**). As the same way, it was observed that pH_c , pH_{ϕ_1} and pH_{ϕ_2} also
297 increased with mixture ratio from 1:1 to 10:1 (respectively from 6.0 to 7.0 for the pH_c value, from 5.0
298 to 6.5 for the pH_{ϕ_1} value and 2.5 to 4.0 for the pH_{ϕ_2} value). At a PPI-TRAG ratio of 1:1, the charges of
299 TRAG chains are supposed to saturate the charges of pea proteins. As the mixture ratio increased,
300 the proteins were in excess, resulting in an increased amount of PPI-PPI aggregates and less complex
301 formation, as previously reported in a PPI-GA interaction study (Liu et al., 2009). A dissolution of the
302 electrostatic complexes at pH_{ϕ_2} occurred when the electrostatic attractive forces declined between
303 the macromolecules due to the protonation of acid functions of TRAG (pH 1.50-2.50). All complexes
304 were assumed to be dissolved near pH 2.04 as revealed by the absence of OD. The dissolution pH
305 was independent of the mixture ratio.

306 The formation of soluble and insoluble complexes occurred at a PPI-GAC mixture ratio of 2:1 at pH
307 4.50 and 4.05, respectively (**Figure 1A**). The increase in turbidity continued up to pH 3.49 reaching
308 the maximal OD value. This value corresponded to the optimal pH value for the maximum formation
309 of PPI-GAC complexes. At pH_{ϕ_2} (2.97), the OD decreased because of the dissociation of the formed
310 complexes. This dissociation would be explained by the protonation of carboxylic acid groups,
311 preventing the association with amino groups of proteins due to electrostatic interactions. Together
312 with the increase in biopolymer ratio, a shift of the optimal pH value was observed. This event was
313 explained by the increase in NH_3^+/COO^- ratio in the protein/polysaccharide mixture. The maximum
314 OD for pH_{opt} was obtained at a ratio of 2:1. It could be assumed that it corresponded to the optimal
315 ratio/ pH_{opt} couple for the maximum formation of PPI-GAC complexes obtained (**Figure 7B**). The
316 results are in accordance with other studies (Liu et al., 2009). A shift of pH_{opt} was also observed
317 towards higher pH values with the increase in mixture ratio from 1:1 to 10:1 (**Figure 1B**).

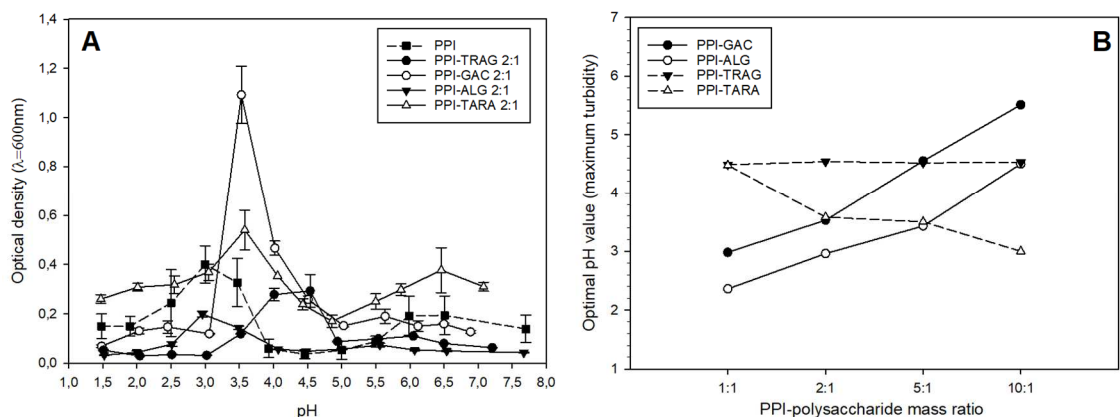
318 In PPI-ALG mixture at a ratio of 2:1, the critical events attributed to the formation of soluble and
319 insoluble complexes were identified at pH 5.59 (pH_c) and 4.04 (pH_{ϕ_1}), respectively, and the optimal
320 biopolymer interactions occurred at pH 2.96 (pH_{opt}) (**Figure 1A**). Together with the increase in
321 biopolymer mixture ratio, the critical pH values shifted towards higher pHs (**Figure 1B**). A strong
322 decrease in OD at $pH < pH_{opt}$ was observed, indicating the occurrence of a partial dissolution of the
323 formed complexes. The maximum OD at pH_{opt} increased from 0.15 at a PPI-ALG ratio of 1:1 to 0.48 at
324 a PPI-ALG ratio of 5:1 (**Figure 7C**). By comparing the different ratios, the 5:1 ratio showed the
325 maximum OD at pH_{opt} value. It suggests that this ratio was considered as the optimal condition to the
326 production complex coacervates from PPI-ALG couple.

327 Overall, the pH_{opt} increased progressively with the increase in mixture ratio for the case of
 328 polyanionic polysaccharide. According to the literature, pH_{opt} values increase with the mixture ratio
 329 until a maximum value is reached after which the OD reached a plateau with further increases in
 330 biopolymer mixture ratio (Klemmer et al., 2012).

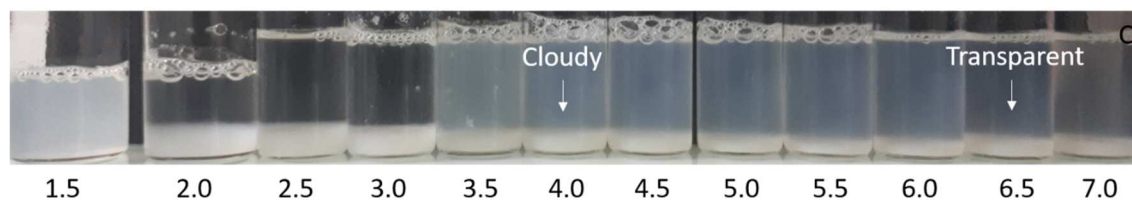
331 Regarding PPI-TARA mixtures, the critical events associated with the formation of complex
 332 coacervates were identified only at ratios of 1:1 and 2:1 (**Figure 1A, 7D**). The optimal biopolymer
 333 interaction occurred at pH 4.48 and 3.58, respectively. Regarding the evolution of pH_{opt} , a shift of
 334 pH_{opt} was observed in **Figure 1B**. The behavior was different from other protein-polysaccharide
 335 mixtures, as the pH_{opt} decreased with the increase of PPI-TARA ratio. As the ratios increased from
 336 5:1, the turbidity profile of PPI-TARA mixtures was similar to that of homogeneous PPI. Although the
 337 latter ratios presented a profile similar to that of PPI alone, the OD of the profile decreased with
 338 increasing mixture ratios. For example, for ratios of 5:1 and 10:1 ratios and homogenous PPI at pH
 339 5.50, the OD was respectively of 0.295, 0.157, and 0.088. This observation suggests an increase in
 340 protein solubility in the presence of tara gum.

341 The magnitude of the increase was dependent on the nature of the polysaccharide involved and the
 342 mixture ratio. Comparing gum tragacanth, gum arabic and sodium alginate, it seemed that the pH_{opt}
 343 decreased with the negative net charge of the polysaccharide. Previous studies have shown that the
 344 pH tends to plateau at higher biopolymer ratios (Klemmer et al., 2012).

345



346



347

348 *Figure 1: A) Curves of the mean turbidity of PPI-TRAG, PPI-GAC, PPI-ALG and PPI-TARA mixtures at a 2:1 ratio according to*
 349 *the pH. B) Critical pH value (pH_{opt}) according to the mass ratio of mixtures of PPI and different polysaccharides (GAC, ALG,*
 350 *TRAG, TARA). C) Appearance of PPI-TRAG at a 2:1 mixing ratio as a function of pH.*

351

352

353 3.2.Zeta potential

354 The zeta potential analysis allows an understanding of the formation and stability of coacervates
355 formed by electrostatic interactions between oppositely charged proteins and polysaccharides.
356 Changes in zeta potential were investigated according to the pH during the same acid titration as the
357 turbidity profile (pH 7.0-2.0), and according to mixture ratio (1:1-10:1).

358 PPI showed a cationic nature at pH values less than 4.80 because of the protonation of the amino
359 groups ($-NH_3^+$, theoretic pKa of about 9.4) while it had an anionic nature at pH values greater than 4.8
360 due to the deprotonation of carboxyl groups (COO^- , theoretic pKa of about 2.5 to 4.5) (Jones and
361 McClements, 2010) (**Figure 2A**). It was admitted that the pKa could change locally depending on the
362 structure of the protein. The isoelectric point (IEP; pI) of commercial pea globulins is known to be in
363 the 4.5-5 pH range, which is consistent with our values (Adebiyi and Aluko, 2011; Cuevas-Bernardino
364 et al., 2018).

365 Tragacanth gum, arabic gum and sodium alginate showed a negative zeta potential, the absolute
366 value of which increased as the pH increased (**Figure 2A**). Like for other anionic biopolymer, the
367 deprotonation of carboxylic groups occurred with the increasing of pH. At higher pH values, the zeta
368 potential no longer changed.

369 Tragacanth gum, like arabic gum, showed a relatively strong polyelectrolyte behavior with a
370 maximum zeta potential of -28,5 mV at pH > 5.0 and approached a neutral zeta potential at pH < 2.0
371 (ZP= -2.7 mV). Structurally, the major fraction of Arabic gum (89% of the total; 280 kDa) consists of a
372 β -(1-3)-galactopyranose backbone highly branched with β -(1-6)-galactopyranose residues
373 terminating in arabinose and glucuronic acid and/or 4-O-methyl-glucuronic acid units (i.e. carboxylic
374 groups from glucuronic acid units) only at the terminus of each branch). This provides the
375 arabinogalactan with its anionic nature. Arabic gum is known to contain about 15-16% of glucuronic
376 acid units (Osman et al., 1993).

377 Tragacanth gum consisted in two fractions: the water-soluble fraction (composed of tragacanthin)
378 and the water insoluble fraction (composed of bassorin). Tragacanthin, a pectic component, is
379 composed of a chain of α -(1-4)-linked D-galacturonic acid units, some of which being replaced at O-3
380 by β -D-xylopyranosyl units and some of them being terminated with D-Galactose or L-Fucose.
381 Bassorin is reported as a neutral, highly branched arabinogalactan (of type II) comprising (1-6)- and
382 (1-3)- linked core chains containing galactose and arabinose (both in the form of furanose and
383 pyranose) and side groups of (1-2)-, (1-3)- and (1-5)-linked arabinose units occurring as
384 monosaccharides or oligosaccharides (Kora and Arunachalam, 2012).The galacturonic acid content
385 varies from 10 to 30% per weight in dry matter depending on the species (Balaghi et al., 2011).

386 Tara gum had a low negative zeta potential between -8 and 0 mV for the pH range tested (**Figure 2A**).
387 The absence of ionisable (acidic or basic) groups allowed the gum to maintain neutrality, and
388 therefore a pKa value estimate was not applicable. Tara gum, unlike most types of anionic
389 polysaccharides (pectin, carrageenan, etc...), is considered a non-ionic polysaccharide. The main
390 chain of the structure consists of β -(1,4)-mannose units with galactose with α -(1,6)-linked branches
391 with a mannose-to-galactose ratio of 3:1 (Barbosa et al., 2019). Its structure is mainly composed of
392 hydroxyl groups, resulting in its neutral nature. It has been demonstrated that other gums such as
393 Guar, Konjac, locust bean gums, also known as gluco- and galactomannans, have the same profile
394 (Barbosa et al., 2019).

395 Sodium alginate showed the highest negative value of zeta potential. Manuacol LD (the commercial
396 sodium alginate used) has been described by Horniblow et al. as a sodium alginate with a molecular
397 weight of 145 kDa and a galacturonic acid - mannuronic acid ratio of 38:62 (Horniblow et al., 2016).
398 Thus, alginate possesses larger carboxylic acid extremities, explaining the higher maximum zeta

399 potential values compared to arabic gum and tragacanth gum, due to differences in their polymeric
400 structures.

401 A charge neutralization could be assumed since the addition of anionic polysaccharides is known to
402 induce to cationic protein adsorption via an electrostatic attraction at pH 3.00-3.50.

403 Regarding PPI-TRAG mixtures, all mixture ratios showed intermediate zeta potentials between those
404 of the two separate biopolymers in solution (**Figure 2B**). As the net charge of biopolymer mixture is
405 closed to zero, the formation of complex coacervation occurred.

406 Therefore, the IEP was used to represent the pH at which the zero net charge of a biopolymer
407 mixture was achieved, and the influence of biopolymer mixture ratios on the IEP is shown in **Figure**
408 **2B, C, D, E**. The electrophoretic mobility corresponded to the mean of electrophoretic mobility of
409 unbound PPI and polysaccharides and that of PPI-polysaccharide complex coacervates. At a mixture
410 ratio of 1:1, the electrophoretic mobility obtained from PPI-TRAG mixture was different from the
411 isoelectric point of PPI alone, decreasing from pH 4,8 (PPI alone) to 3,0 (PPI-TRAG mixture). The
412 mixture showed surface charges similar to those of TRAG with zeta potentials remaining negative
413 within the pH range of 7.0-3.0. As the mixture ratio increased, the isoelectric point changed towards
414 higher pH values, reaching a pH value of 4.20 at a mixture ratio of 10:1, close to homogeneous PPI
415 solution (**Figure 2F**). Similar results have been reported for the association of tragacanth gum with
416 whey proteins (Raoufi et al., 2016). Moreover, a high zeta potential magnitude of soluble complexes,
417 observed at pH > 4.50, has highlighted an electrostatic repulsion in the system, preventing protein
418 precipitation (Klassen and Nickerson, 2012).

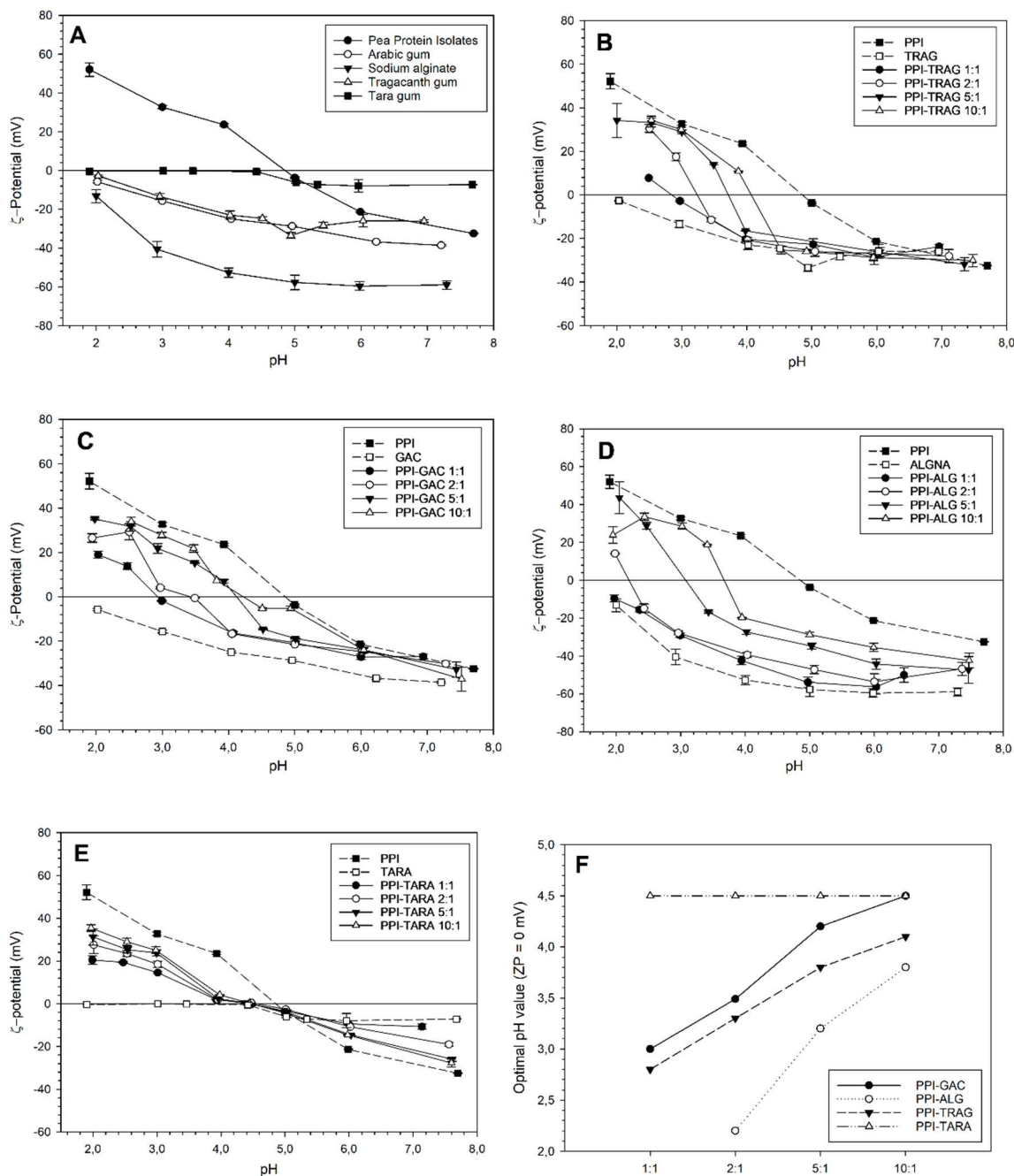
419 The electrophoretic mobility of the PPI-GAC mixture at a ratio of 1:1 was electrophoretically neutral
420 at pH 3.00 (**Figure 2C**). Electrophoretic mobility measurements of the PPI-GAC mixture at a ratio of
421 2:1 allowed estimating the net neutral surface charge of the formed complexes at pH 3.49, which
422 was consistent with the pH_{opt} of the system. Data were in accordance with similar studies of PPI-GAC
423 complexes (Liu et al., 2009). At a higher pH, the formed complexes carried a net negative charge
424 when the charge contribution from GA was superior to that of PPI. In contrast, at a lower pH, a net
425 positive charge of the complexes was found when the positive charge contribution from PPI
426 dominated due to the protonation of glucuronic acid residues of GA., the IEP of the mixture shifted
427 with a trend similar to PPI-TRAG mixtures when the mixture ratio increased towards higher pH values
428 (**Figure 2F**).

429 The addition of ALG to PPI shifted the pH of the net neutrality from 4.80 (homogeneous PPI) to 1.47
430 at a PPI-ALG ratio of 1:1 (**Figure 2D**). As shown by Klemmer et al., an electrophoretic mobility profile
431 similar to that of the homogeneous ALG solution was identified, and a negative charge was retained
432 within the examined pH range (Klemmer et al., 2012). The increased protein content in the mixture
433 ratio inducing a shift towards higher pHs (**Figure 2F**). The pHs of the net neutrality were close to pH_{opt}
434 values at a corresponding biopolymer mixture ratio, suggesting that at pHs close to pH_{opt} , charge
435 neutralisation occurred.

436 In contrast, the pH corresponding to the net neutrality did not shift with the addition of TARA
437 regardless of the mixture ratio (**Figure 2E, F**). The pH of the net neutrality was equivalent to 4.50 in
438 all mixture ratios. The maximum zeta potential value increased with the ratio, due to the increasing
439 addition of proteins, which were charged, to the mixture. Thus, the evolution of the zeta potential in
440 this mixture was mainly due to the amount of PPI added to the mixture.

441 The Charge neutralization can be modulated by altering the charge of one or both biopolymers or by
442 varying the mixture ratios between PPI and polysaccharides. The zeta potential values obtained were

443 due to the contribution of complex coacervates but also to unbound PPI and polysaccharides that
 444 greatly contribute to the measured net charge according to the ratio and the excess of one of the
 445 biopolymers in the mixtures. In all mixture ratios, the zeta potential value of dispersions became
 446 more positive with the decrease in pH from 7.00 to 2.00, suggesting the formation of more positively
 447 charged complexes. For all mixtures, complexes carried a net negative charge at $pH > pI$, whereas at
 448 $pH < pI$, the complexes carried a net positive charge.



449

450

451

452 *Figure 2: Mean zeta potential (mV) of pea protein isolates and polysaccharides (arabic gum, sodium alginate, tragacanth*
 453 *gum and tara gum) (A) and mixtures (PPI-TRAG (B), PPI-GAC (C), PPI-ALG (D) and PPI-TARA (E)) at different ratios according*
 454 *to the pH. Data represents the mean ± standard deviation (n=3). F) Critical pH values according to the mass ratio of PPI and*
 455 *different polysaccharides (GAC, ALG, TRAG, TARA).*

456 **3.3. Pea protein solubility**

457 In this section, the pH-dependent solubility profile of the soluble PPI-polysaccharide complexes
458 formed was explored.

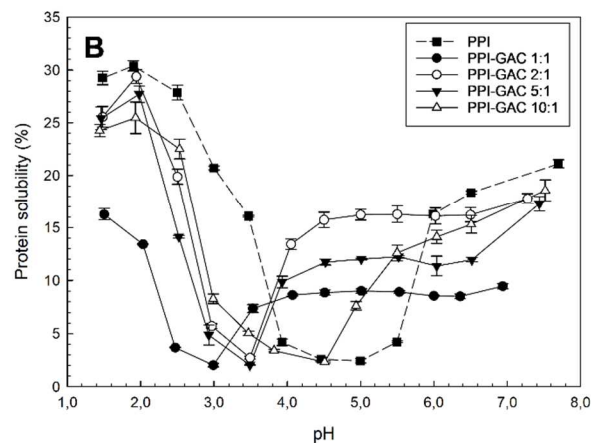
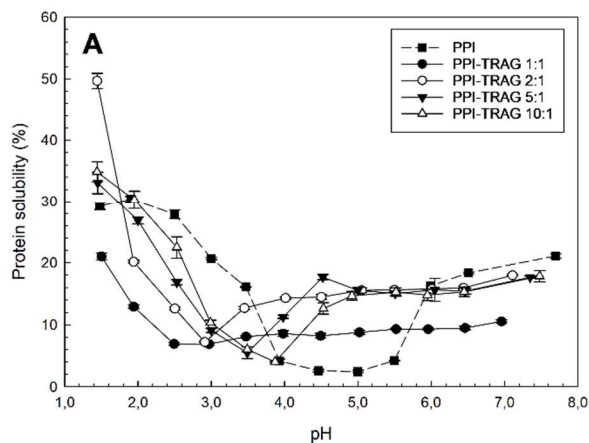
459 The PPI solubility profile showed a downward trend with a decrease from 22% at pH 7.00 to its
460 minimum (3%) at pH 4.5, corresponding to the protein IEP (**Figure 3A**). It was followed by an increase
461 in solubility with progressive pH decreases. Similar protein solubility profiles have been reported with
462 commercial PPI (Guo et al., 2019).

463 Regarding PPI-TRAG mixtures, the presence of TRAG increased the PPI protein solubility at pH 4.50
464 (pI) from 2.5% (homogeneous PPI) to 14.6% (PPI-TRAG ratio of 2:1) (**Figure 3A**). This trend was
465 explained by the decrease of PPI self-aggregation with addition of tragacanth gum. This has also been
466 reported for pea protein - pectin mixtures ((Warnakulasuriya et al., 2018). Also, the pH for PPI
467 minimum solubility was shifted from 4.50 to 3.50 as the PPI-TRAG mixture ratio decreased from 10:1
468 to 2:1. This phenomenon was in agreement with the previously observed phase behavior. This has
469 previously been demonstrated by the protein-polysaccharide complexes formation at pH less than
470 4.00, increasing protein solubility in an acid pH range (Guo et al., 2019).

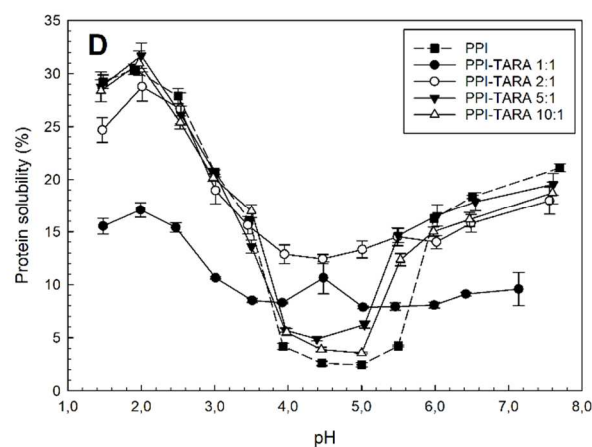
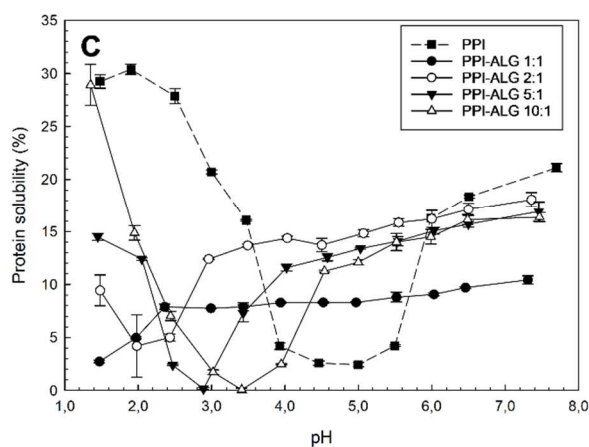
471 Similarly, the addition of GAC and ALG to PPI mixed systems induced a shift in the minimum solubility
472 from PPI alone (**Figure 3B, C**). It has been suggested that this shift could be linked to soluble and
473 insoluble complexes formation (Liu et al., 2010). Also, a shift of pH range from which a minimal
474 solubility occurred has been observed towards more acidic pHs as the polysaccharide amount
475 increased in soy protein-carrageenan complexes (Molina Ortiz et al., 2004). The addition of ALG to
476 PPI resulted in a loss of solubility at PPI-ALG ratio of 5:1 and 10:1 (0,15 and 0,07% respectively),
477 because protein precipitation dominated in the system. Overall, the complexation with anionic
478 polysaccharides appears to shift the pH of the minimum protein solubility towards more acid pH
479 values (Guo et al., 2019; Klassen et al., 2011; Liu et al., 2010). PPI-GAC and PPI-TRAG mixtures shared
480 a similar trend in pH-dependent protein solubility profile in terms of pH value shifting (**Figure 3E**).
481 Differences observed between the PPI-ALG, PPI-GAC and PPI-TRAG mixtures could be related to the
482 charge of the polysaccharide (Klassen et al., 2011). As reported by Klassen *et al.*, alginate and
483 carrageenan differ in their surface charge, leading to a difference in canola protein precipitation, ι -
484 carrageenan being more likely to induce canola protein precipitation (Klassen et al., 2011). Similarly,
485 the tendency of polysaccharides tested in this study to form complexes with PPI was dependent on
486 the surface charge of polysaccharides, with alginate > arabic gum > tragacanth gum.

487 Regarding PPI-TARA mixtures, since TARA is a non-ionic polysaccharide, the association with PPI plays
488 a minor role. The incompatibility observed was directly correlated with the protein self-association as
489 observed at ratios ranging between 5:1 and 10:1, because they had a profile similar to that of
490 homogeneous PPI (**Figure 3D**). As the PPI-polysaccharide ratio decreased, the protein solubility
491 increased for values greater than or less than pI by limiting PPI self-aggregation. As showed in **Figure**
492 **3E**, the minimum solubility at the different PPI-TARA ratios was close to the pI of PPI because the
493 biopolymers were not charged at this pH. Overall, it has been admitted that the pH and ionic
494 strength only affect protein self-association in protein - non-ionic polysaccharide systems (Syrbe et
495 al., 1998).

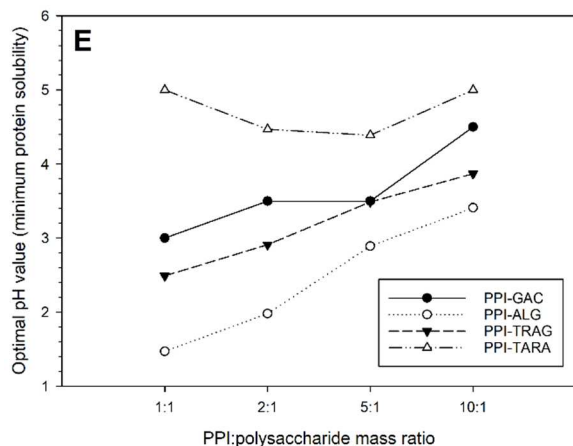
496



497



498



499 *Figure 3: Percentage of protein solubility of the PPI-TRAG (A), PPI-GAC (B), PPI-ALG (C) and PPI-TARA (D) mixtures at*
 500 *different ratios according to the pH. Data represents the mean \pm standard deviation ($n=3$). E) Critical pH values according to*
 501 *the mass ratio of mixtures PPI and different polysaccharides (GAC, ALG, TRAG, TARA) corresponding to the minimum protein*
 502 *solubility.*

503 **3.4. Coacervation yield of concentrated mixtures**

504 PPI-TARA and PPI-TRAG mixtures were prepared at a total biopolymer concentration of 1.0% and
 505 2.0% (w/v), respectively, due to the high viscosity of the gums, while PPI-GAC and PPI-ALG mixtures
 506 were prepared at a concentration of 5.0%. The coacervation yield was obtained from the percentage

507 of protein solubility measured in the supernatant after centrifugation. The coacervation yield was
508 mainly associated with complex coacervation between the pea proteins and the polysaccharides and
509 with the self-aggregation of pea proteins.

510 The yields obtained in the PPI-GAC mixtures were in agreement with the previously performed
511 analyses (turbidity and zeta potential) (**Figure 4B**). The maximum yield corresponded to a mixture
512 ratio of 2:1 at pH 3.50, which was in agreement with the higher OD value obtained in the turbidity
513 analysis. A pH shift was also observed as the mixture ratio increased. However, this shift was not
514 clearly identified as in 0.3% total biopolymer study since the yields seemed to be very close to one
515 another and the maximum yield value obtained did not seem significant.

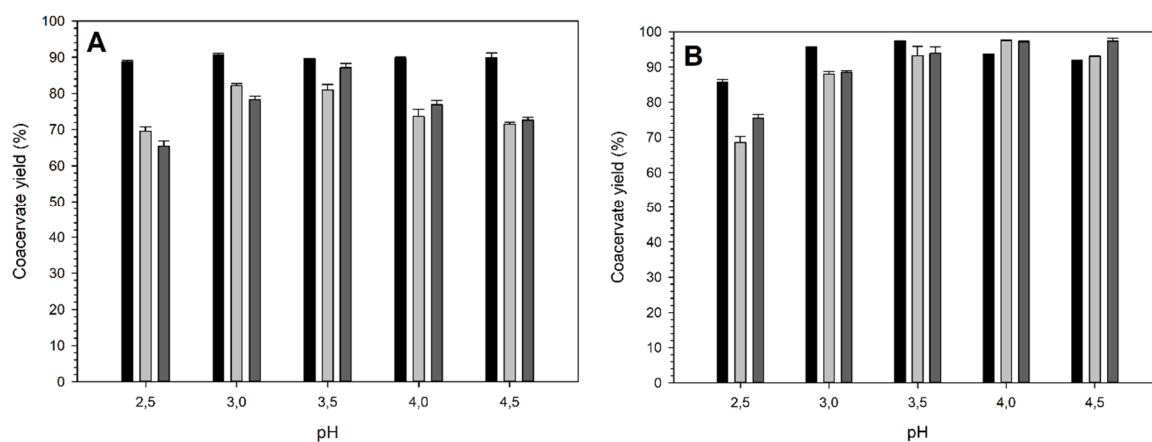
516 Similarly, in the PPI-ALG and PPI-TRAG mixtures, the best yields obtained were respectively for the
517 ratio of 5:1 at pH= 3.50 and for the ratio of 2:1 at pH= 3.0 (**Figure 4A, C**). A shift was also observed as
518 previously reported. However, the results of the PPI-TRAG mixtures differed from those of the
519 turbidity analysis by 0.50 pH unit. The yield was improved in the presence of alginate due to its
520 higher surface charge, compared to PPI-TRAG and PPI-GAC mixtures. In all pea protein -
521 polysaccharide mixtures, the pH value corresponding to maximal value yield shifted towards higher
522 pHs. This shift of pH values was similar to the pH shift limit in the turbidity and zeta potential studies,
523 showing that the pH required for the maximum production of coacervates shifted as the pea protein
524 - anionic polysaccharide mixture ratio increased.

525 In contrast, the coacervation yield obtained for PPI-TARA mixtures seemed to correspond to a PPI
526 self-aggregation mechanism as tara gum was considered as a non-ionic polysaccharide (**Figure 4D**).
527 The presence of TARA appeared to decrease the aggregation, since the solubility increased (or the
528 obtained yield decreased).

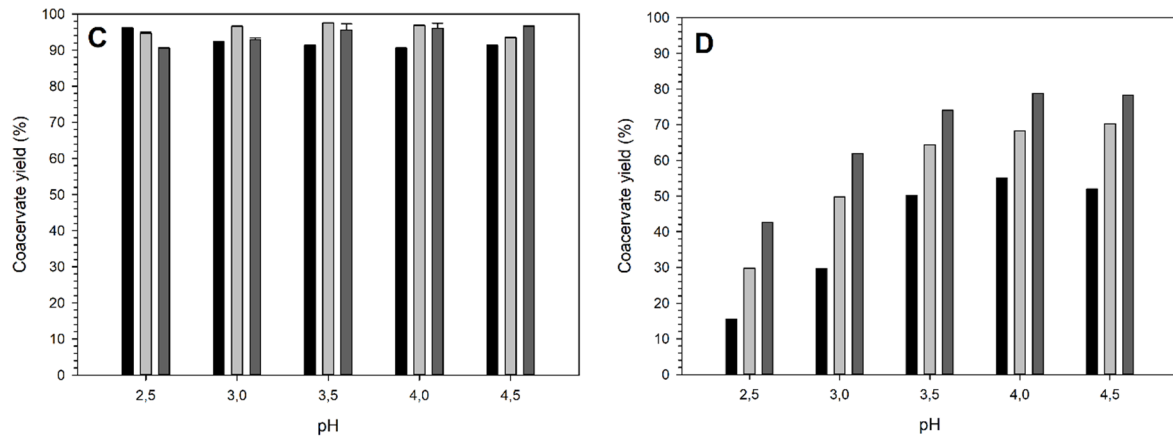
529 The higher yield obtained with independent ratios corresponded to the neutral net charge value
530 obtained in the zeta potential analysis. Differences in maximal complex coacervation yield values
531 obtained between PPI-anionic polysaccharides could be due to the polysaccharide surface charge
532 (alginate > arabic gum > tragacanth gum) as observed in the previous protein solubility study.

533

534



535



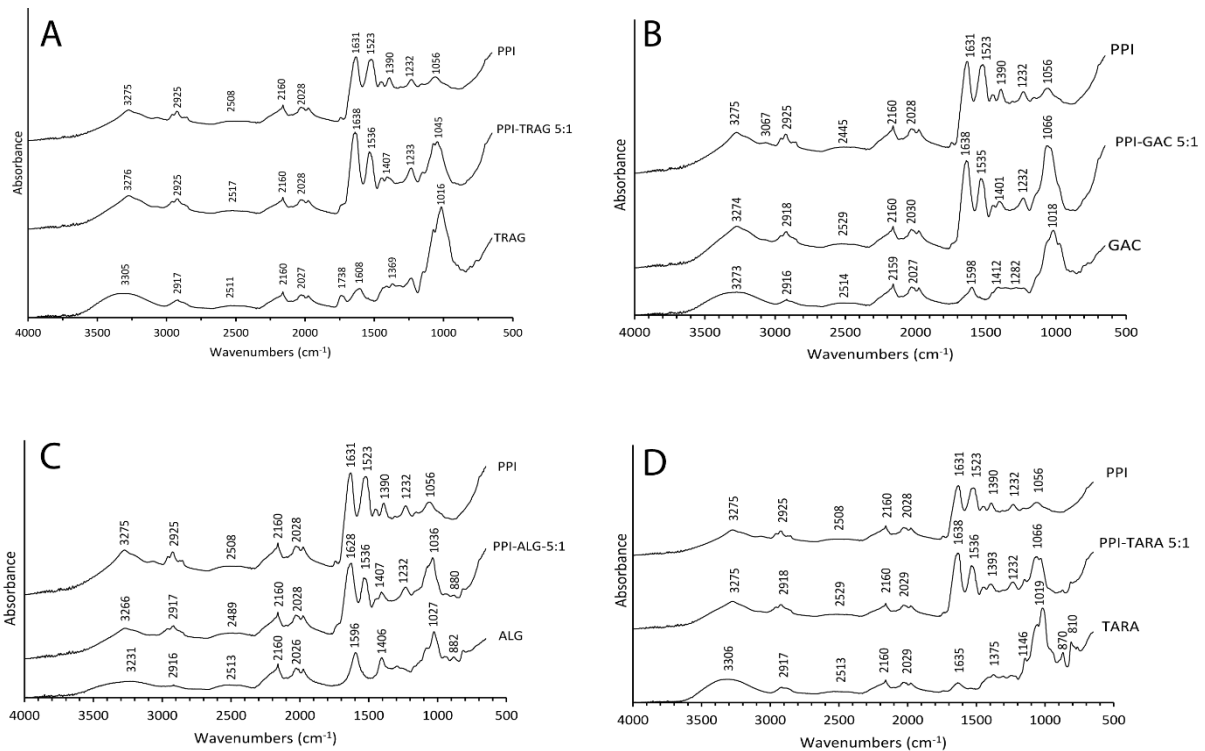
536

537 *Figure 4: Coacervation yield of pea protein – polysaccharide mixtures (PPI-TRAG (A), PPI-GAC (B), PPI-ALG (C) and PPI-TARA*
 538 *(D)) at ratios of 2:1 (black), 5:1 (light grey) and 10:1 (dark grey) determined based on the protein solubility in concentrated*
 539 *solutions.*

540

541 3.5. FTIR analysis

542 Previously prepared complex coacervates were spray-dried to obtain microparticles. Then, they were
 543 characterized by FTIR and observed by SEM.



544

545 *Figure 5: FTIR spectra of the PPI-TRAG (a), PPI-GAC (b), PPI-ALG (c) and PPI-TARA (d) mixtures prepared at PPI:*
 546 *Polysaccharide ratio of 5 :1.*

547 The FTIR analysis provides information on the structure of proteins and polysaccharides and their
 548 interactions in the mixture. Molecularly, the interactions of functional groups can lead to the appearance of
 549 new bands and to changes in absorption band or location in the FTIR spectra. **Figure 5** shows the FTIR
 550 spectra of raw materials as well as the dried protein-polysaccharide mixtures.

551 Regarding the tragacanth gum spectrum, the broad band at 3305 cm^{-1} could be attributed to stretching
552 vibrations of hydroxyl- groups in the gum (**Figure 5A**). The bands at $2800\text{-}3000\text{ cm}^{-1}$ corresponded to
553 asymmetric and symmetric stretching vibrations of C-H groups. The broad band at 2160 cm^{-1} was related to
554 the carbonyl species of the gum. The peak at 1608 cm^{-1} could be attributed to the characteristic
555 asymmetrical stretching of carboxylate group. The symmetrical stretching of carboxylate groups could be
556 associated with the bands present in the zone of 1369 cm^{-1} (Kora and Arunachalam, 2012). The peaks of the
557 region of 1016 cm^{-1} were associated with the fingerprint region of carbohydrates.

558 The spectrum of arabic gum showed an absorption band at $3290\text{-}3305\text{ cm}^{-1}$ corresponding to -OH hydrogen
559 bonded groups, characteristics of glucosidic rings (**Figure 5B**). The peak at 2916 cm^{-1} was due to the
560 presence of sugars, galactose, arabinose, rhamnose, alkane with C-H stretching and aldehyde C-H. The
561 peaks at 1598 and 1412 cm^{-1} were respectively related to COO^- symmetric and asymmetric stretching. The
562 peak at 1018 cm^{-1} was associated with alkene C-H bends (Daoub et al., 2018).

563 The spectrum of sodium alginate showed characteristic bands corresponding to carboxylic, ether and
564 hydroxyl groups (**Figure 5C**). The peak at 1406 and 1596 cm^{-1} were attributed to symmetric and asymmetric
565 -COO^- stretching vibration, while the peak at 3231 cm^{-1} was related to the stretching vibration of -OH
566 groups (Nayak and Pal, 2011).

567 The spectrum of tara gum showed characteristic peaks at 810 and 870 cm^{-1} , which are associated with the
568 presence of $\alpha\text{-D-galactopyranose}$ units and $\beta\text{-D-mannopyranose}$ units (**Figure 5D**). The peaks at 1019 and
569 1146 cm^{-1} corresponded to the C-O stretching vibration of pyranose rings. (Figueiro et al., 2004). The peak
570 at 1375 cm^{-1} was attributed to -CH_2 and C-OH symmetrical deformations. The peak at 1635 cm^{-1} was
571 associated with the association with water. The broad peaks ranging from 2800 to 3000 cm^{-1} were related
572 to the O-H and C-H stretching vibration.

573 Regarding pea proteins, a strong -OH contraction vibration band and a C-H stretching band were
574 respectively observed at 3275 cm^{-1} and 2925 cm^{-1} (**Figure 5**). The stretching or bending of C=O at 1631 cm^{-1} ,
575 N-H deformation and C-N stretching at 1523 cm^{-1} and C-N stretching at 1232 cm^{-1} corresponded to amide I
576 (high content of β -sheet structures), II and III, respectively (Aguilar-Vázquez et al., 2018). The peak of amide
577 I was due to a high content of β -sheet structures (Wang et al., 2011). The peak at 1056 cm^{-1} corresponded
578 to C-O vibration stretching.

579 Regarding the spectra of raw materials and coacervates, the functional groups present in the coacervates
580 closely resembled the functional groups of pea proteins and the polysaccharides involved. The domination
581 of PPI structure was clearly established in the spectrum of PPI-TRAG complexes due to the higher protein
582 ratio (5:1), but it was different from that of each individual biopolymer.

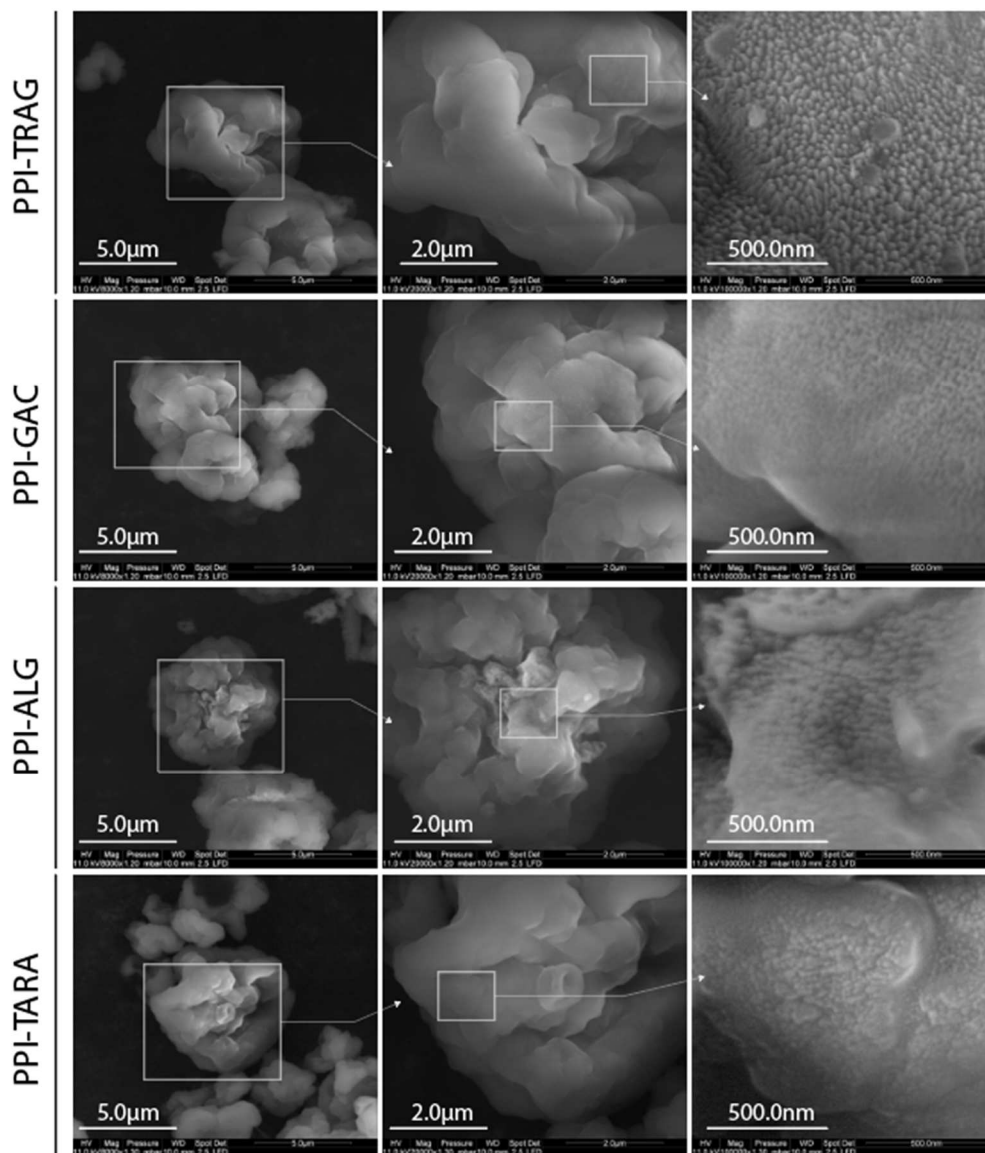
583 Regarding PPI-TRAG complexes, the peaks corresponded to amide I of PPI shifted from 1631 to 1638 cm^{-1}
584 (**Figure 5A**). The peaks related to amide II and III were shifted respectively from 1523 and 1232 cm^{-1} to 1536
585 and 1233 cm^{-1} . The shifting of amide peaks could be explained by conformational changes in α -helix
586 structures towards β -sheets configuration (Mousazadeh et al., 2018). Moreover, a decrease of the
587 intensity of amide II and III peaks (respectively at 1536 cm^{-1} and 1407 cm^{-1}) was observed in the complexes
588 compared to the separate pea protein solution due to a decrease of free functional groups. The
589 disappearance of peaks corresponding to TRAG, especially at 1635 cm^{-1} , could also point out the presence
590 of interactions between the two biopolymers (Mousazadeh et al., 2018). In addition, the disappearance of
591 the peak might be attributed to the excess of protein in the mixture. The "fingerprint region" of PPI-TRAG
592 coacervates showed a broad band ($1100\text{-}950\text{ cm}^{-1}$) which could be due to the superposition of PPI (1056 cm^{-1}
593 corresponding to carboxylate stretching vibration) and TRAG (peak 1073 and 1016 cm^{-1} , C-O-C stretching
594 vibration) spectra. This involved the establishment of electrostatic interactions between pea proteins and
595 the gum leading to the formation of coacervates.

596 Overall, the carbonyl-amide region was affected during the formation complex coacervates. The
597 coacervates did not show the symmetric -COO^- stretching vibrations (1608 cm^{-1}) found for TRAG. A shift of
598 wavenumbers was observed in amide peaks towards higher values compared to native PPI and could be
599 explained by the establishment of electrostatic interactions between the amino groups of PPI and the
600 carboxylic groups of TRAG. This phenomenon have also been observed in gelatin-carboxymethylcellulose
601 complex formation (Duhoranimana et al., 2017) . The same observations were made for PPI-GAC mixture.
602 In the case of PPI-ALG mixture, a shift of the amide I peak wavenumber was observed towards lower value
603 compared to native PPI (1631 cm^{-1} to 1628 cm^{-1}).

604

605 3.6. ESEM observations

606 A systematic examination of the surface morphology of the spray-dried microparticles was achieved by
607 Environmental Scanning Electron Microscopy (ESEM) (**Figure 6**). The average size of microparticles ranged
608 between 2 and $10\mu\text{m}$. The aggregation of sub-micron particles on larger particles was observed. The
609 microparticles showed a predominantly spherical shape with a rough surface and concavities. These
610 wrinkles/distorsions have been attributed to the uneven shrinkage of the particles during the drying
611 process with rapid evaporation of water (Eratte et al., 2015; Sheu and Rosenberg, 1998). The appearance of
612 these microstructures has been observed by various authors in the preparation of microparticles using a
613 spray-drying process (Gharsallaoui et al., 2010; Nesterenko et al., 2012; Pierucci et al., 2007). These
614 wrinkles could improve the release properties of microparticles due to a greater surface area. Details of the
615 microparticle surface showed a regular polymeric network, without any porous structure, suggesting a high
616 integrity of the encapsulating materials. However, some nanometric irregularities were observed at the
617 surface of some particles, also modulating the release of potential encapsulated compounds (Jun-xia et al.,
618 2011) (**Figure 6**, PPI-TRAG $\times 100,000$). These irregularities could be described as a network composed of
619 organized “fibrillar-like” strands of 25-75 nm. These nanostructures are similar to those observed during
620 pea protein gelation in the presence of calcium chloride (Munialo et al., 2014). However, the morphology of
621 pea protein-based particles obtained using spray-drying process has not been clearly described in the
622 literature at a nanometric scale since the use of a coating during SEM observations could cover the
623 roughness and porosities on the particle surface due to their small dimensions. The metal-coated particle
624 surface looked smoother than it actually was (Conforto et al., 2015). Since this roughness was found on the
625 various protein-polysaccharide mixtures, it could be assumed that it could be linked with the nature of the
626 protein instead of the nature of the polysaccharide.



627

628 *Figure 6: SEM observations (left to right: x8,000; x20,000; x100,000) of spray-dried PPI-TRAG, PPI-GAC, PPI-ALG and PPI-*
 629 *TARA coacervates prepared at a ratio of 5:1.*

630 **4. Conclusion**

631 This study compared the ability of commercial tragacanth gum to form complex coacervates with pea
 632 proteins to three other polysaccharides: arabic gum, sodium alginate and tara gum. Tragacanth gum, arabic
 633 gum and sodium alginate formed effectively complex coacervates with PPI. Complex coacervation is highly
 634 dependent on the pH as well as the nature and concentration of the polysaccharide used. This study
 635 showed the optimum parameters for complex coacervation between the pea protein and tragacanth gum
 636 with a maximum interaction at a PPI/TRAG ratio of 2:1 at pH 4.5. The zeta potential analysis, that allowed
 637 performing the preformulation study, identified a pH shifting from 2.8 to 4.0 as the PPI-TRAG mixture ratio
 638 increased from 1:1 to 10:1. Overall, the pH values of critical structure-forming events, especially pH_{opt}
 639 values, were shifted towards higher pHs as the protein content increased in all PPI-polysaccharide mixtures.
 640 Moreover, the pH-dependent protein solubility profile was shifted towards more acid pH values as the
 641 biopolymer ratio decreased. For more concentrated solutions, there was a correspondence of pH values
 642 between optimal yield and the neutral net charge value obtained in the zeta potential analysis of 0.3% w/v
 643 solutions. Differences in yield obtained could be due to the polysaccharide surface charge (alginate > arabic

644 gum > tragacanth gum). Compared to arabic gum, tragacanth gum appears to be a good alternative since its
645 properties are similar in association with PPI. Regarding PPI-TARA mixtures, the possible formed complexes
646 were dependent on pea protein self-aggregation since tara gum was considered a non-ionic polysaccharide.
647 The electrostatic interaction between proteins and polysaccharide backbones were verified by FTIR. The
648 surface morphology of the generated microparticles was studied by SEM. The spray-dried microparticles
649 maintained a spherical shape and a surface without fracture. An observation at nanometric scale showed
650 fibrillar-like structures which could be of interest to further studies in other fields of coacervation. Based on
651 our findings, PPI associated with different anionic polysaccharides could be used in the area of
652 microencapsulation.

653 **Declaration of competing interest**

654 The authors are not aware of any affiliations, memberships, funding or financial holdings that could affect
655 the objectivity of this article.

656 **Acknowledgements**

657 We thank Dr Egle Conforto from the CCA platform of La Rochelle University for her assistance in SEM
658 observation. This work was financially supported by INNOV'IA and IDCAPS (La Rochelle, France).

659

660 **5. References**

661 Adebisi, A.P., Aluko, R.E., 2011. Functional properties of protein fractions obtained from commercial
662 yellow field pea (*Pisum sativum* L.) seed protein isolate. *Food Chemistry* 128, 902–908.

663 Aguilar-Vázquez, G., Loarca-Piña, G., Figueroa-Cárdenas, J.D., Mendoza, S., 2018. Electrospun fibers
664 from blends of pea (*Pisum sativum*) protein and pullulan. *Food Hydrocoll.* 83, 173–181. Anderson,
665 D.M.W., Bridgeman, M.M.E., 1985. The composition of the proteinaceous polysaccharides exuded by
666 astragalus microcephalus, A. Gummifer and A. Kurdicus—The sources of turkish gum tragacanth.
667 *Phytochemistry* 24, 2301–2304.

668 Aryee, F.N.A., Nickerson, M.T., 2012. Formation of electrostatic complexes involving mixtures of lentil
669 protein isolates and gum Arabic polysaccharides. *Food Research International* 48, 520–527.

670 Balaghi, S., Mohammadifar, M.A., Zargaraan, A., 2010. Physicochemical and Rheological
671 Characterization of Gum Tragacanth Exudates from Six Species of Iranian Astragalus. *Food Biophysics*
672 5, 59–71.

673 Balaghi, S., Mohammadifar, M.A., Zargaraan, A., Gavlighi, H.A., Mohammadi, M., 2011.
674 Compositional analysis and rheological characterization of gum tragacanth exudates from six species
675 of Iranian Astragalus. *Food Hydrocolloids* 25, 1775–1784.

676 Barbosa, J.A.C., Abdelsadig, M.S.E., Conway, B.R., Merchant, H.A., 2019. Using zeta potential to study
677 the ionisation behaviour of polymers employed in modified-release dosage forms and estimating
678 their pKa. *International Journal of Pharmaceutics: X* 1, 100024.

679 Boye, J., Zare, F., Pletch, A., 2010. Pulse proteins: Processing, characterization, functional properties
680 and applications in food and feed. *Food Res. Int.* 43, 414–431.

681 Conforto, E., Joguet, N., Buisson, P., Vendeville, J.-E., Chaigneau, C., Maugard, T., 2015. An optimized
682 methodology to analyze biopolymer capsules by environmental scanning electron microscopy.
683 *Materials Science and Engineering: C* 47, 357–366.

684 Daoub, R.M.A., Elmubarak, A.H., Misran, M., Hassan, E.A., Osman, M.E., 2018. Characterization and
685 functional properties of some natural Acacia gums. *Journal of the Saudi Society of Agricultural*
686 *Sciences* 17, 241–249.

687 Ducel, V., Richard, J., Saulnier, P., Popineau, Y., Boury, F., 2004. Evidence and characterization of
688 complex coacervates containing plant proteins: application to the microencapsulation of oil droplets.
689 *Colloids and Surfaces A: Physicochemical and Engineering Aspects* 232, 239–247.

690 Duhoranimana, E., Karangwa, E., Lai, L., Xu, X., Yu, J., Xia, S., Zhang, X., Muhoza, B., Habinshuti, I.,
691 2017. Effect of sodium carboxymethyl cellulose on complex coacervates formation with gelatin:
692 Coacervates characterization, stabilization and formation mechanism. *Food Hydrocolloids* 69, 111–
693 120.

694 Figueiro, S., Goes, J., Moreira, R., Sombra, A., 2004. On the physico-chemical and dielectric properties
695 of glutaraldehyde crosslinked galactomannan–collagen films. *Carbohydrate Polymers* 56, 313–320.

696 Gharsallaoui, A., Saurel, R., Chambin, O., Cases, E., Voilley, A., Cayot, P., 2010. Utilisation of pectin
697 coating to enhance spray-dry stability of pea protein-stabilised oil-in-water emulsions. *Food*
698 *Chemistry*, 5th Conference on Water in Food 122, 447–454.
699

700 Ghayempour, S., Montazer, M., Mahmoudi Rad, M., 2016. Encapsulation of Aloe Vera extract into
701 natural Tragacanth Gum as a novel green wound healing product. *International Journal of Biological*
702 *Macromolecules* 93, 344–349.

703 Ghorbani Gorji, S., Ghorbani Gorji, E., Mohammadifar, M.A., Zargaraan, A., 2014. Complexation of
704 sodium caseinate with gum tragacanth: Effect of various species and rheology of coacervates.
705 *International Journal of Biological Macromolecules* 67, 503–511.

706 Guo, Q., Su, J., Yuan, F., Mao, L., Gao, Y., 2019. Preparation, characterization and stability of pea
707 protein isolate and propylene glycol alginate soluble complexes. *LWT – Food Science and Technology*
708 101, 476–482.

709 Horniblow, R.D., Latunde-Dada, G.O., Harding, S.E., Schneider, M., Almutairi, F.M., Sahni, M., Bhatti,
710 A., Ludwig, C., Norton, I.T., Iqbal, T.H., Tselepis, C., 2016. The chelation of colonic luminal iron by a
711 unique sodium alginate for the improvement of gastrointestinal health. *Mol. Nutr. Food Res.* 60,
712 2098–2108.

713 Jain, A., Thakur, D., Ghoshal, G., Katare, O.P., Shivhare, U.S., 2016. Characterization of
714 microcapsulated β -carotene formed by complex coacervation using casein and gum tragacanth.
715 *International Journal of Biological Macromolecules* 87, 101–113.

716 Jones, O.G., McClements, D.J., 2010. Functional Biopolymer Particles: Design, Fabrication, and
717 Applications. *Comprehensive Reviews in Food Science and Food Safety* 9, 374–397.

718 Kayitmazer, A.B., 2017. Thermodynamics of complex coacervation. *Adv. Colloid Interface Sci.* 239,
719 169–177.

720 Klassen, D.R., Elmer, C.M., Nickerson, M.T., 2011. Associative phase separation involving canola
721 protein isolate with both sulphated and carboxylated polysaccharides. *Food Chemistry* 126, 1094–
722 1101.

723 Klassen, D.R., Nickerson, M.T., 2012. Effect of pH on the formation of electrostatic complexes within
724 admixtures of partially purified pea proteins (legumin and vicilin) and gum Arabic polysaccharides.
725 Food Research International 46, 167–176.

726 Klemmer, K.J., Waldner, L., Stone, A., Low, N.H., Nickerson, M.T., 2012. Complex coacervation of pea
727 protein isolate and alginate polysaccharides. Food Chemistry 130, 710–715.

728 Kora, A.J., Arunachalam, J., 2012. Green Fabrication of Silver Nanoparticles by Gum Tragacanth (
729 Astragalus gummifer): A Dual Functional Reductant and Stabilizer. Journal of Nanomaterials 2012, 1–
730 8.

731 Lan, Y., Ohm, J.-B., Chen, B., Rao, J., 2020. Phase behavior and complex coacervation of concentrated
732 pea protein isolate-beet pectin solution. Food Chem. 307, 125536.

733 Liu, S., Elmer, C., Low, N.H., Nickerson, M.T., 2010. Effect of pH on the functional behaviour of pea
734 protein isolate–gum Arabic complexes. Food Research International 43, 489–495.

735 Liu, S., Low, N.H., Nickerson, M.T., 2009. Effect of pH, Salt, and Biopolymer Ratio on the Formation of
736 Pea Protein Isolate–Gum Arabic Complexes. J. Agric. Food Chem. 57, 1521–1526.

737 Molina Ortiz, S.E., Puppo, M.C., Wagner, J.R., 2004. Relationship between structural changes and
738 functional properties of soy protein isolates–carrageenan systems. Food Hydrocolloids 18, 1045–
739 1053.

740 Mousazadeh, M., Mousavi, M., Askari, G., Kiani, H., Adt, I., Gharsallaoui, A., 2018. Thermodynamic
741 and physicochemical insights into chickpea protein-Persian gum interactions and environmental
742 effects. International Journal of Biological Macromolecules 119, 1052–1058.

743 Munialo, C.D., van der Linden, E., de Jongh, H.H.J., 2014. The ability to store energy in pea protein
744 gels is set by network dimensions smaller than 50nm. Food Research International 64, 482–491.

745 Nayak, A.K., Pal, D., 2011. Development of pH-sensitive tamarind seed polysaccharide–alginate
746 composite beads for controlled diclofenac sodium delivery using response surface methodology.
747 International Journal of Biological Macromolecules 49, 784–793.

748 Nazarzadeh Zare, E., Makvandi, P., Tay, F.R., 2019. Recent progress in the industrial and biomedical
749 applications of tragacanth gum: A review. Carbohydrate Polymers 212, 450–467.

750 Nesterenko, A., Alric, I., Silvestre, F., Durrieu, V., 2012. Influence of soy protein’s structural
751 modifications on their microencapsulation properties: α -Tocopherol microparticle preparation. Food
752 Research International 48, 387–396.

753 Nur, M., Ramchandran, L., Vasiljevic, T., 2016. Tragacanth as an oral peptide and protein delivery
754 carrier: Characterization and mucoadhesion. Carbohydrate Polymers 143, 223–230.

755 Osman, M.E., Williams, P.A., Menzies, A.R., Phillips, G.O., 1993. Characterization of commercial
756 samples of gum arabic. J. Agric. Food Chem. 41, 71–77.

757 Pierucci, A.P.T.R., Andrade, L.R., Farina, M., Pedrosa, C., Rocha-Leão, M.H.M., 2007. Comparison of
758 alpha-tocopherol microparticles produced with different wall materials: pea protein a new
759 interesting alternative. J Microencapsul 24, 201–213.

760 Raoufi, N., Kadkhodae, R., Phillips, G.O., Fang, Y., Najafi, M.N., 2016. Characterisation of whey
761 protein isolate-gum tragacanth electrostatic interactions in aqueous solutions. *Int J Food Sci Technol*
762 51, 1220–1227.

763 Sheu, T.-Y., Rosenberg, M., 1998. Microstructure of Microcapsules Consisting of Whey Proteins and
764 Carbohydrates. *J Food Science* 63, 491–494.

765 Syrbe, A., Bauer, W.J., Klostermeyer, H., 1998. Polymer Science Concepts in Dairy Systems—an
766 Overview of Milk Protein and Food Hydrocolloid Interaction. *International Dairy Journal* 8, 179–193.

767 Tamnak, S., Mirhosseini, H., Tan, C.P., Tabatabaee Amid, B., Kazemi, M., Hedayatnia, S., 2016.
768 Encapsulation properties, release behavior and physicochemical characteristics of water-in-oil-in-
769 water (W/O/W) emulsion stabilized with pectin–pea protein isolate conjugate and Tween 80. *Food*
770 *Hydrocolloids* 61, 599–608.

771 Toews, R., Wang, N., 2013. Physicochemical and functional properties of protein concentrates from
772 pulses. *Food Research International* 52, 445–451.

773 Turgeon, S.L., Beaulieu, M., Schmitt, C., Sanchez, C., 2003. Protein–polysaccharide interactions:
774 phase-ordering kinetics, thermodynamic and structural aspects. *Current Opinion in Colloid &*
775 *Interface Science* 8, 401–414.

776 Wang, C., Jiang, L., Wei, D., Li, Y., Sui, X., Wang, Z., Li, D., 2011. Effect of Secondary Structure
777 determined by FTIR Spectra on Surface Hydrophobicity of Soybean Protein Isolate. *Procedia Eng.* 15,
778 4819–4827.

779 Warnakulasuriya, S., Pillai, P.K.S., Stone, A.K., Nickerson, M.T., 2018. Effect of the degree of
780 esterification and blockiness on the complex coacervation of pea protein isolate and commercial
781 pectic polysaccharides. *Food Chemistry* 264, 180–188.

782 Weinbreck, F., de Vries, R., Schrooyen, P., de Kruif, C.G., 2003. Complex Coacervation of Whey
783 Proteins and Gum Arabic. *Biomacromolecules* 4, 293–303.